Investigation of Effective Restraining Force on Rib Fracture Risk Reduction for Elderly Occupant in Frontal Collision

Yoshiki Takahira, Yu Hayashi, Toshiyuki Kasai, Shigeki Hayashi, Yasuaki Kosugi
Yann Ngueveu, Andrea Lucchini-Gilera

Abstract A chest model was generated to represent the rib cortical bone material property and thickness of a 70-year-old person. The chest model was applied to THUMS V4.1 occupant models in four body sizes: midsize male, small female, large male and overweight female. Frontal collision simulations were performed to predict rib fracture risks using three-specification restraint systems with different restraining balances for the shoulder belt and airbag. Simulation results show that higher Body Mass Index, rather than sex difference, is related to a higher number of rib fractures in elderly occupants of the driver's seat. The contact force from shoulder belt to anterior chest was greater than that from the airbag and was one of the possible factors causing rib fractures. The load limiter of the seat belt reduced the contact force to the chest, but it allowed further head forward displacement. The study results indicate that the combination of low load limiter and early airbag constraint was effective for elderly occupants with various body types.

Keywords Elderly occupant, Human body FE model, Rib fracture, Vehicle frontal collision simulation.

I. INTRODUCTION

In recent years, the proportion of elderly people involved in road traffic injuries and deaths has increased, particularly in Japan and European countries [1-2]. It has been reported that the most common cause of death for elderly occupants in frontal collision was chest injury [3]. Furthermore, the crash safety performance for various occupants, such as female, obese person and so on, has come into focus recently. Adams *et al.* reported that statistical analysis of FARS accident data showed that female occupants tended to have a higher mortality rate than male occupants [4]. Ejima *et al.* analyzed the trauma computed tomography of accident patients and reported that occupants with a higher BMI were more likely to have lower rib fractures [5]. In crash safety regulations and in New Car Assessment Programs (NCAP), anthropomorphic test dummies (ATDs) are used to evaluate an occupant's risk of rib fractures. Recently, THOR ATDs with improved biofidelity compared to conventional ATDs have been used, and elderly female and obese male ATDs have also been developed [6]. However, ATDs do not properly predict the rib fractures of the human body. On the other hand, human body FE models (HBMs) reproduce the structure of the human body anatomically and directly simulate rib fractures based on bone strain. In a previous study, the mechanism of rib fractures in elderly midsize male occupants (AM50) in frontal collision using human body FE model THUMS was investigated [7]. The results showed that rather than the anterior-posterior deflection commonly thought to be the indicator for rib fracture, the main injury mechanism is from torsion and superior-inferior bending of rib, mainly caused by increase of vertical chest loading from shoulder-belt contact force due to upper body flexion.

The objective of this study is to investigate the effective restraining force on the rib fracture risk reduction for elderly occupants with various body types. The vehicle frontal collision simulations were performed using the occupant models of AF05, AM95 and a newly developed overweight female model, in addition to AM50. The overweight female model represents recent data on American average elderly female, with a body mass index (BMI) of 29.3 and a torso shape statistically developed by the International Center for Automotive Medicine (ICAM) [8-9]. The influence of the occupant body type and the restraining balance for shoulder belt and airbag to the chest impact responses and rib fracture patterns were investigated using these models.

Y. Takahira (e-mail: yoshiki_takahira@mail.toyota.co.jp; tel: +81 50 3192 0175) is Assistant Manager, Y. Hayashi is Engineer, T. Kasai is Group Manager, S. Hayashi and Y. Kosugi are Project Managers in Toyota Motor Corporation, Japan. Y. Ngueveu is Senior Engineer and A. Lucchini-Gilera is Senior Manager in Toyota Motor Europe, Belgium.

II. METHODS

The simulations were performed using FE models. LS-DYNA™ Version 971 solver was used for the FE analysis. It is developed by Livermore Software Technology Corporation (US). The FE models consisted of occupant models and the vehicle sled model, including seat and restraint systems.

Occupant Model

The THUMS Version 4.1 AM50, AF05 and AM95 occupant models and a recently developed overweight female model, as shown in Fig. 1 and Table I, were used in the vehicle frontal collision simulations. The AM50 model corresponds to a midsize male, with a height of 177 cm and a weight of 76 kg. The AF05 model corresponds to a small size female, with a height of 153 cm and a weight of 50 kg. The AM95 model corresponds to a large size male, with a height of 189 cm and a weight of 102 kg. The overweight female model corresponds to a midsize female of 70 years old (yo), with a height of 161 cm and a weight of 76 kg. The overweight female model was developed by morphing AF05 model with reference to the geometry data that were generated statistically based on the trauma computed tomography of accident patients, as shown in Fig. 2. The cross-sectional area of the ribs, which was the focus of this study, was larger as the body height was higher. The models describe the anatomical features of the human body, including the major skeletal parts, articular ligaments, brain, internal organs and other soft tissue parts. THUMS' mechanical responses were validated for various loading cases using PMHS test data [10-13].

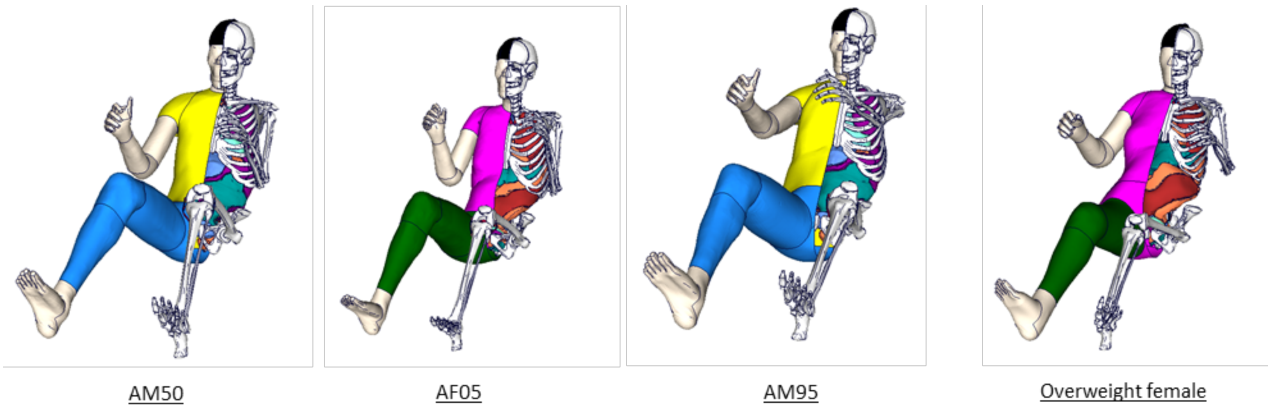

Fig. 1. THUMS occupant models.

TABLE I
SPECIFICATION OF OCCUPANT MODELS

Body size	Height [cm]	Weight [kg]	BMI	Area of rib cortical bone [cm²] *
AM50	177	76	24.3	24
AF05	153	50	21.4	17
AM95	189	102	28.6	27
Overweight female	161	76	29.3	19

* Example of 5th rib outermost

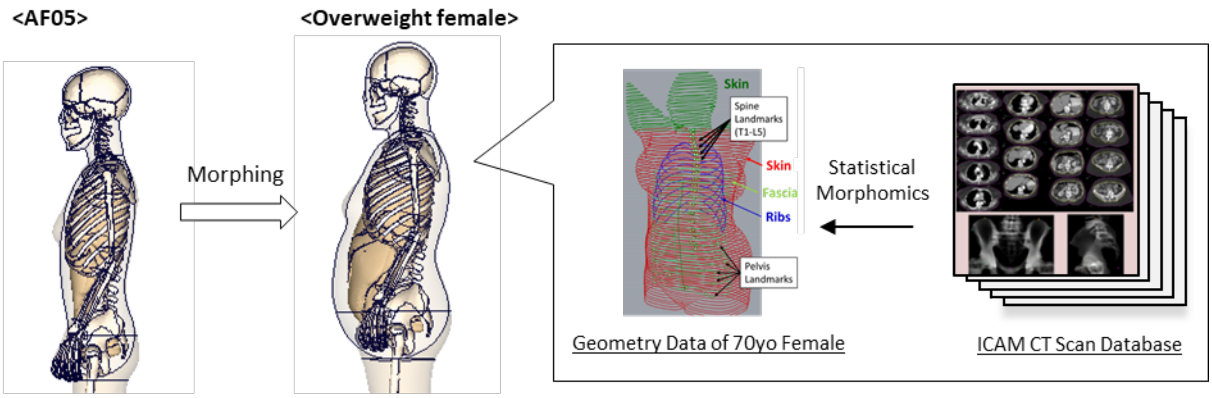

Fig. 2. Overview of Overweight female model.

Age-related Model Preparation

THUMS models were developed as a representative of 30yo. In this study, they were assumed to be 35yo. To represent THUMS 70yo, the ribcage characteristics of 70yo human developed in the previous study were applied to the ribcage part in THUMS 35yo, as shown in Fig. 3 [7]. The cortical bone stress-strain curves scaled yield and fracture points from 35yo to 70yo and reduced fracture strain by 37%. The cortical bone thickness of ribs and clavicles was reduced by 28% to represent those of 70yo, based on the measurement of rib cross-sectional area. The cortical bone thickness of the sternum was reduced from 1 mm (35yo) to 0.4 mm (70yo).

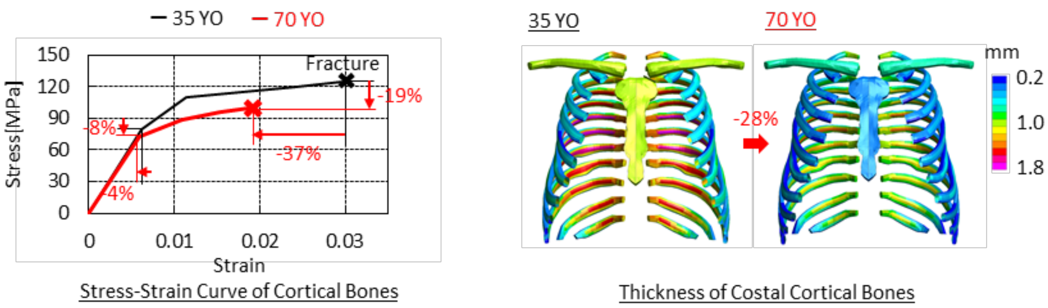

Fig. 3. Age-related parameters of ribcage characteristics.

Vehicle Frontal Collision Simulation Model

Figure 4 shows the simulation model used in this study. The model was used to validate the occupant kinematics, impact response and patterns of rib fracture of THUMS 70yo model by comparing with PMHS tests [7]. It represents a prototype midsize sedan with the driver's seat. The interior parts (steering, instrument panel, pedals, seat, seat belt and airbags) that could come into contact with occupants were assumed to be deformable, while the windshield and floor panel were assumed to be rigid. The seat-belt retractor model simulated the functions of a pretensioner and a load limiter. The deployment of the driver airbag (DAB) and knee airbag (KAB) was also simulated. The seat slide position was adjusted to fit a driving posture for each occupant: AM50: neutral; AF05: 10 mm rearward from the front most; AM95: rear most; Overweight female: 30 mm forward from the neutral, for full track length of the seat: 260 mm. An acceleration pulse of a frontal collision at a speed of 56 km/h was applied to the model. The simulation results using THOR ATD model were shown in Table A-I.

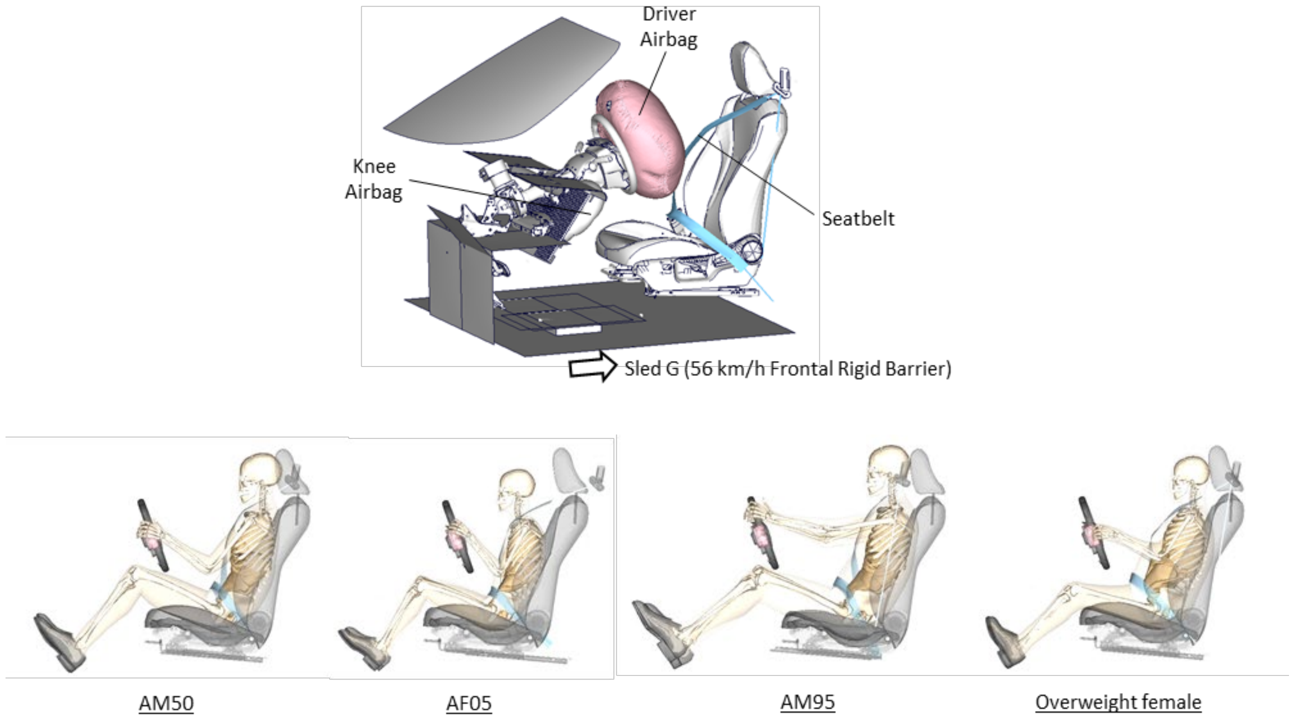

Fig. 4. Vehicle frontal collision model.

Simulation Matrix

A total of 12 simulations were conducted with the parameters: (i) occupant body type as shown in Fig. 4, (ii) specification of the restraint system, as shown in Table II and Fig. 5. Three types of the tentative specification with different restraint balance of the shoulder belt and DAB were prepared. The restraint system of Type A had a base load limiter for the seat-belt retractor and a base DAB. The Type B assumed the load limiter was reduced by 25% compared to Type A. The Type C kept same load limiter as Type B but increased the DAB deployment height by 25% without increase of the volume, and the gas venting was reduced by 25% compared to Type B. However, the characteristics of these three restraint systems are tentative and do not represent actual characteristics.

TABLE II
SIMULATION MATRIX

Body size	Age	Restraint system		
		Type A	Type B	Type C
AM50	70YO	#1	#2	#3
AF05	↑	#4	#5	#6
AM95	↑	#7	#8	#9
Overweight female	↑	#10	#11	#12

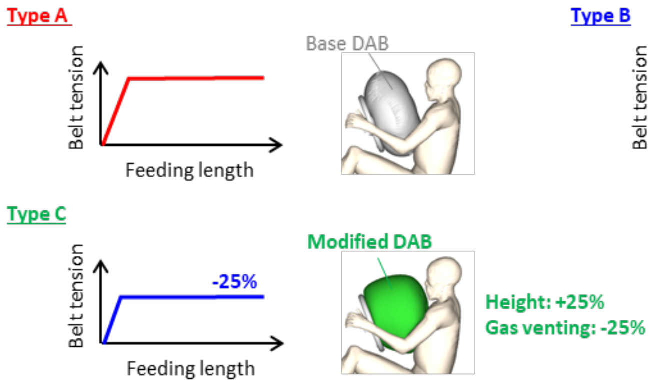

Fig. 4. Specification of restraint systems.

Post-processing of Simulation Result

The 3D coordinate data of all nodes and the strain values of all elements were extracted every 2 milliseconds (ms). Time history data, such as displacement calculated on the selected node and contact force from the shoulder belt and DAB, were output every 0.1 ms. Post-processing software Animator™ and LS-PrePost™ were used to visualize the impact kinematics of the occupant model and to plot the time history curve. The impact kinematics was analyzed in the vehicle coordinate system. The nodal time history data of THUMS anatomical landmarks were output. The landmark points were the head centre of gravity (COG) and T4 thoracic spine, as shown in Fig.65. The chest bone fractures were simulated by the elimination of cortical bone shell elements that reached the fracture strain (plastic strain: 0.011). The number of locations where the cross section was separated by the fracture was counted as the number of bone fractures. Based on the crash safety regulations UN-R94 and UN-R137, the head injury was evaluated with HIC15: 700, and the head bottoming out was evaluated with a 3 ms average acceleration of head COG: 80 G as the reference values.

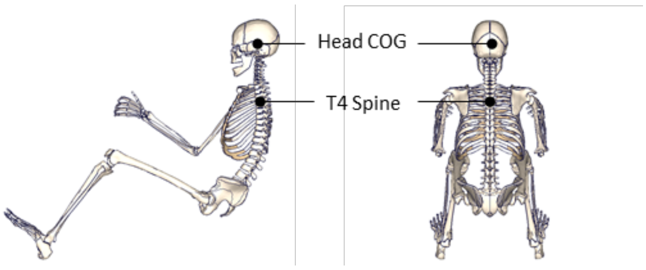

Fig. 6. Landmark points of occupant.

III. RESULTS

Occupant Kinematics

Figure 7 shows the occupant kinematics in a lateral view at the time when the T4 spine forward displacement reached the maximum value with respect to the vehicle. For all driver body types, the largest T4 spine forward movement was observed with Type B restraint system as the belt tension reduced for all drivers' body types. In particular, DABs almost bottomed out for AM95 and overweight female drivers. In Type C, which has a higher DAB deployment height than Type B, the amount of displacement decreased to the same level as or less than that of Type A. In addition, when compared by body type, the amount of displacement of AF05 was the smallest, followed by that of the overweight female and AM50, and that of AM95 was the largest. In other words, the heavier the occupant weight and the further the seat slide from the DAB, the greater amount of forward displacement is predicted.

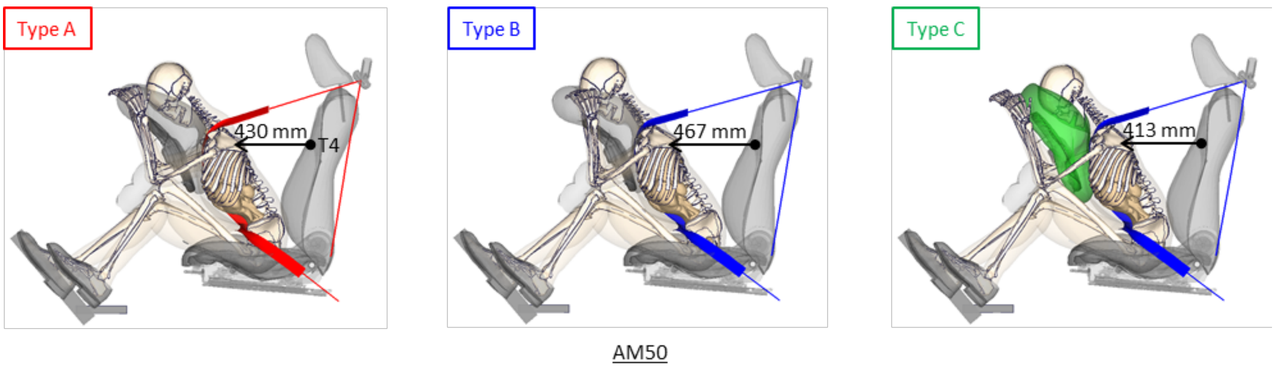

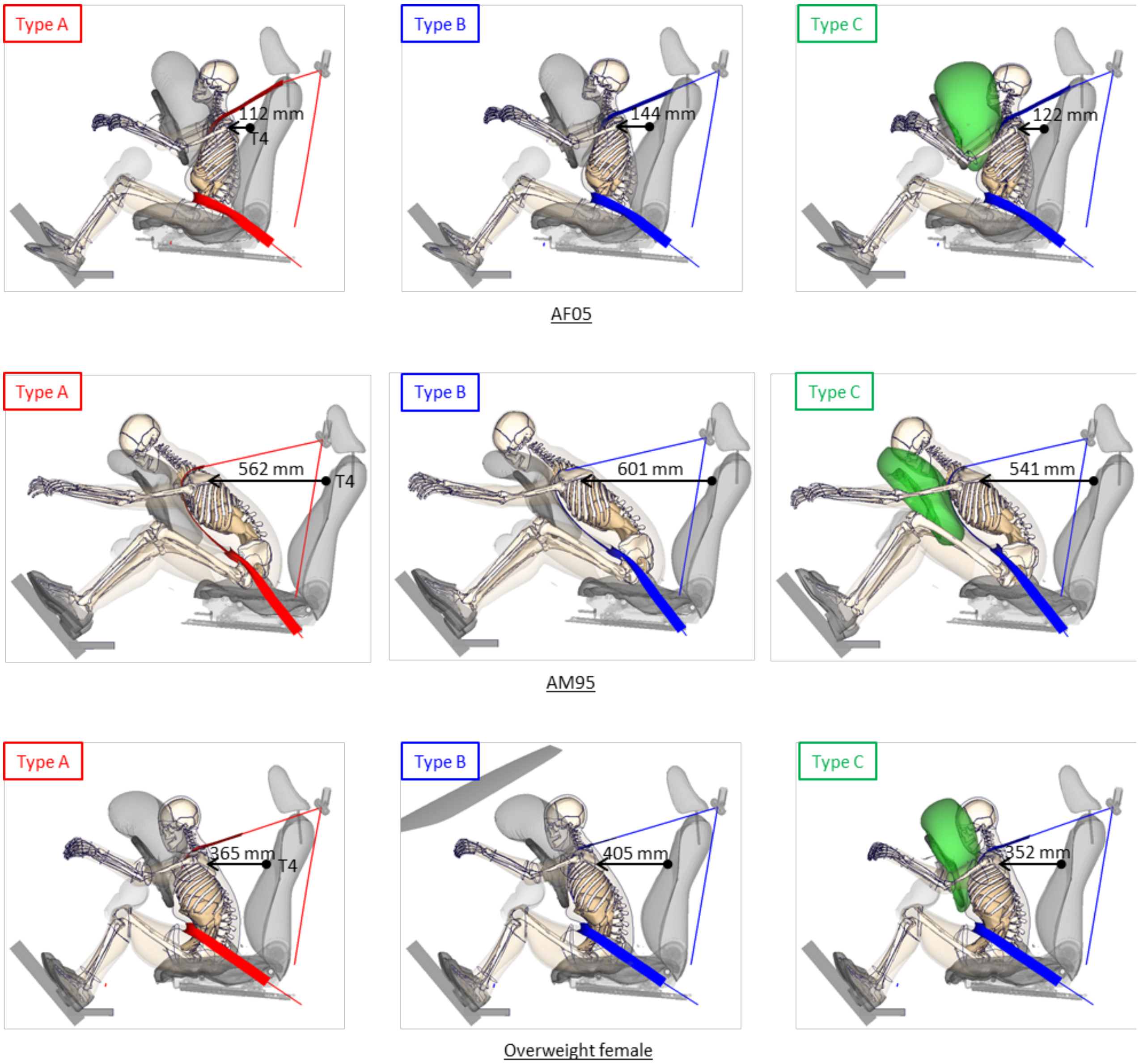

Fig. 7. Occupant kinematics.

Chest Bone Strain and Fracture Pattern

Figure 8 shows the distribution of plastic strain in the chest cortical bone and the location of fracture. In all body types, the magnitude of bone strain and the number of fractures decreased in the order of Type A, Type B, and Type C. The number of fractures of the AM50 occupant model was 5 locations in Type A, 3 locations in Type B, and 0 locations in Type C, mainly in the upper left chest. AF05 model had fewer fractures than AM50 model, with 2 locations each in Type A and Type B and 1 location in Type C. The number of fractures in AM95 model was higher than in AM50 model, with 8 locations in Type A, 7 locations in Type B, and 4 locations in Type C, mainly in the left side of the chest. The number of fractures of overweight female model was 12 locations in Type A and 10 locations each in Type B and Type C, mainly in the right side of the chest, which was the highest among all body types.

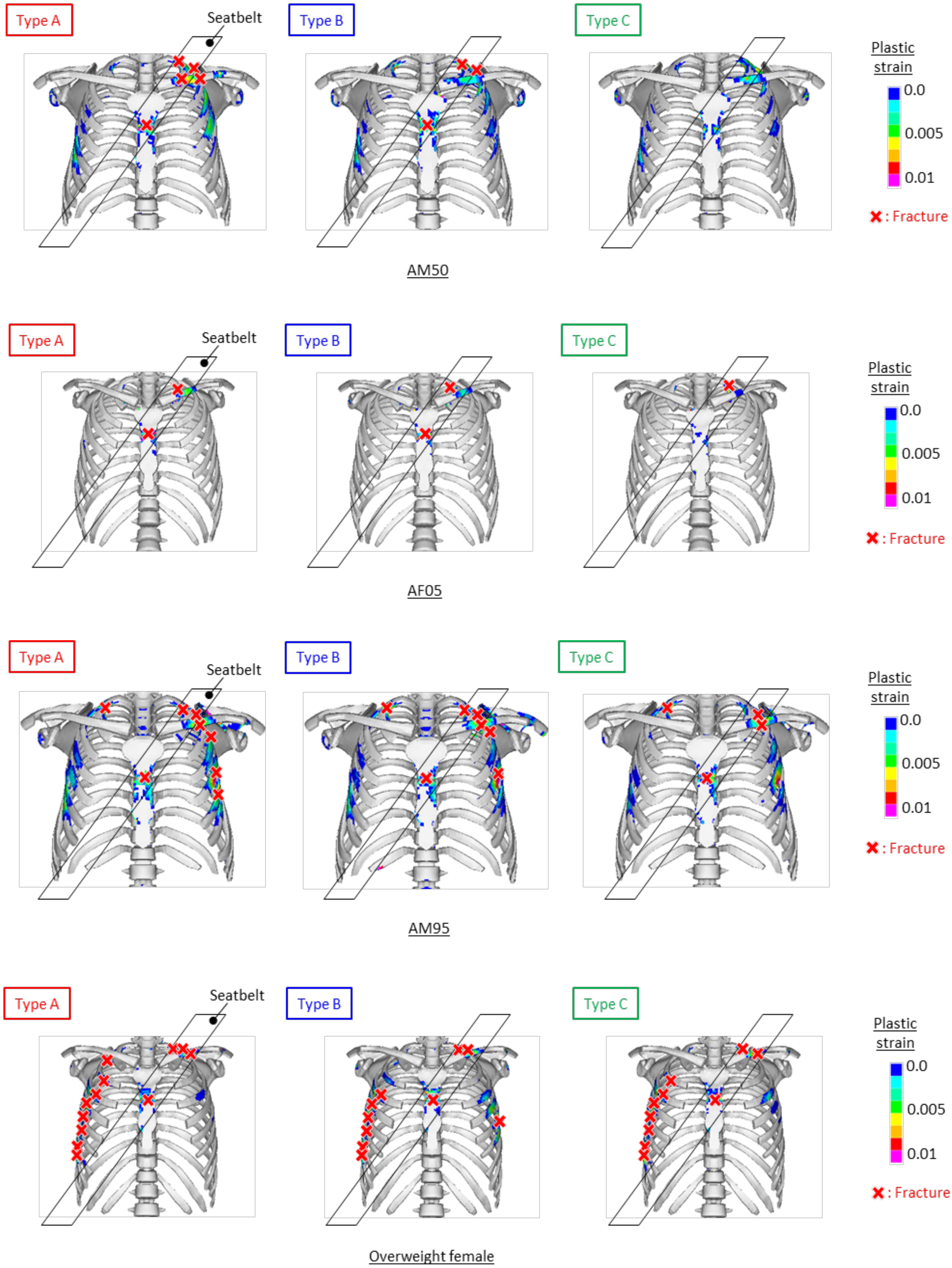

Fig. 8. Plastic strain distribution of rib cortical bone and fracture patterns.

Dynamic Response of Chest

Figure 9 shows the chest force-displacement curves. The vertical axis indicates the contact force applied to the chest from the shoulder belt and DAB, while the horizontal axis indicates the chest (T4) forward displacement. As the chest moved forward, the contact force from the shoulder belt increased. The maximum contact force from the shoulder belt in the Type A restraint system was the lowest at about 4 kN for AF05 model, followed by the same level at about 6 kN for AM50 model and overweight female model, and the highest at about 8 kN for AM95 model. For all body types, Type B, which has reduced seat-belt tension from Type A, reduced the contact force from the shoulder belt but increased the chest displacement. In Type C, which has a higher airbag deployment height, the initial restraint force from the DAB increased, the chest displacement reduced, and the contact force from the shoulder belt decreased, compared to Type B.

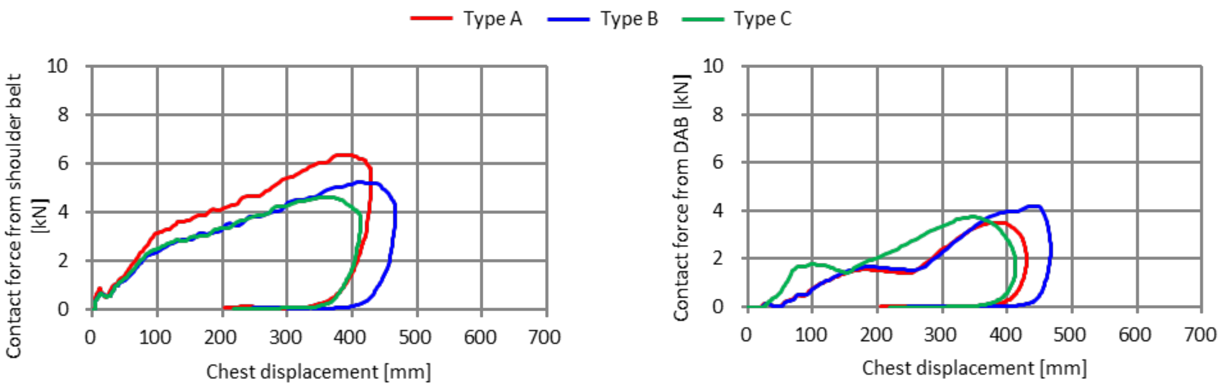

AM50

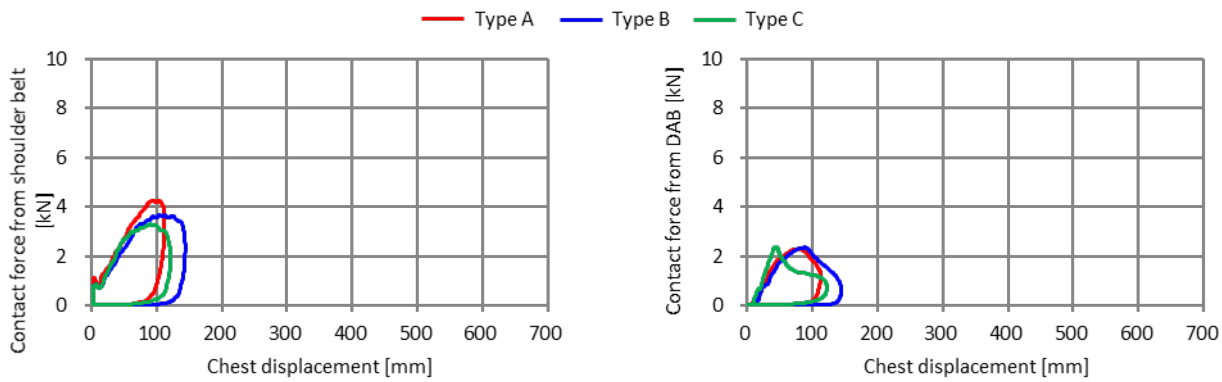

AF05

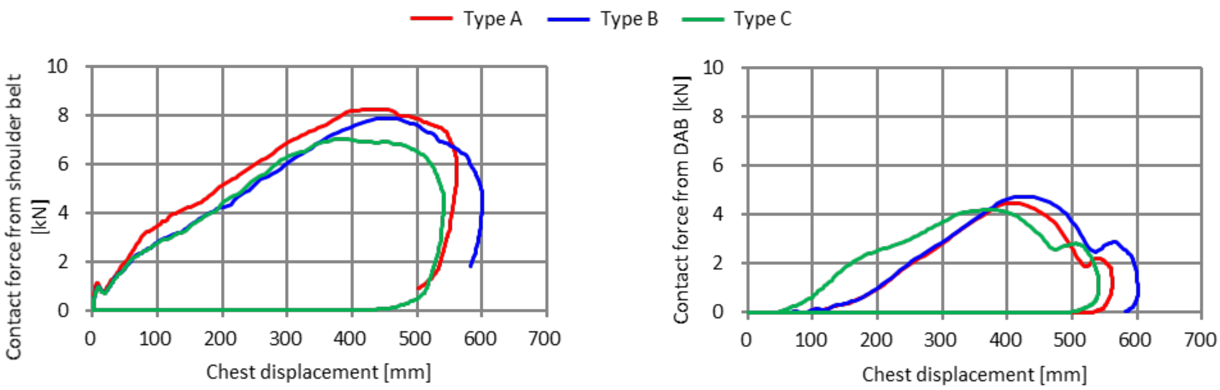

AM95

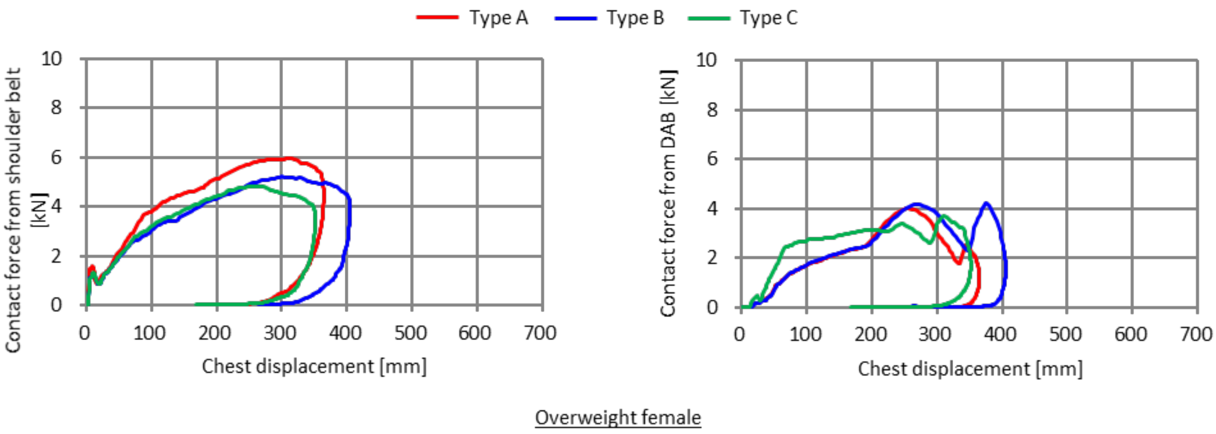

Fig. 9. Shoulder-belt and DAB contact force and T4 displacement curves.

Dynamic Response of Head

Figure 10 shows the head acceleration-displacement curves. The vertical axis indicates the 3 ms average acceleration of head COG, while the horizontal axis indicates the forward displacement of head COG. In Type B, the head displacement increased compared to Type A. For AM50, a sharp acceleration was observed as the head bottomed out at maximum displacement. On the other hand, in Type C, the head G increased at an early timing, the head overall displacement decreased, and the maximum G reduced. In AF05 and overweight female models, the peak level of head G was almost the same in all types of restraint system.

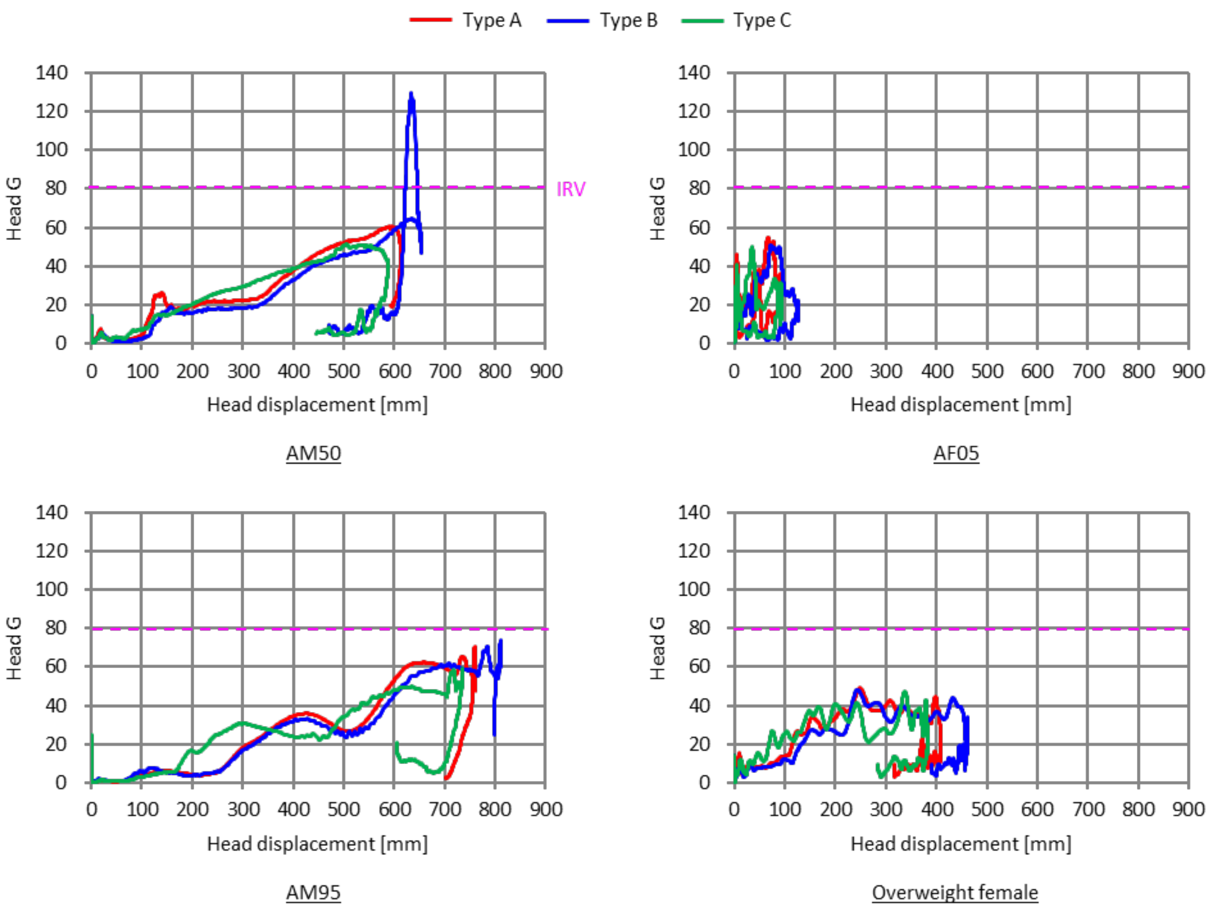

Fig. 10. Head acceleration and head displacement curves.

Injury Measurement

Table III shows a summary of occupant injury indicators: i) the number of rib fractures, ii) HIC15, and iii) the 3 ms average acceleration of the COG of the head. The restraint system Type B reduced the number of rib fractures in all body types compared to Type A, however HIC15 and 3 ms G exceeded the reference values for AM50 occupants. Type C had fewer fractures in AM50, AF05 and AM95 than Type B, but overweight female had the same number of fractures as Type B. In Type C, HIC15 and 3 ms G of AM50 also decreased to below the reference values.

TABLE III
OCCUPANT INJURY INDICATOR

i) Number of rib fractures

Body size	BMI	Age	Restraint system		
			Type A	Type B	Type C
AM50	24.3	70YO	**5**	**3**	**0**
AF05	21.4	↑	**2**	**2**	**1**
AM95	28.6	↑	**8**	**7**	**4**
Overweight female	29.3	↑	**12**	**10**	**10**

0-2 2-4 ≧ 5

ii) HIC15

Body size	BMI	Age	Restraint system		
			Type A	Type B	Type C
AM50	24.3	70YO	**388**	**913**	**264**
AF05	21.4	↑	**259**	**243**	**180**
AM95	28.6	↑	**446**	**506**	**317**
Overweight female	29.3	↑	**158**	**146**	**122**

＜700 ≧ 700

iii) Head 3 ms G

Body size	BMI	Age	Restraint system		
			Type A	Type B	Type C
AM50	24.3	70YO	**60.6**	**130**	**51.3**
AF05	21.4	↑	**54.6**	**51.0**	**50.0**
AM95	28.6	↑	**70.1**	**73.7**	**59.1**
Overweight female	29.3	↑	**49.1**	**48.1**	**47.2**

＜80 ≧ 80

IV. DISCUSSION

The impact response and injury risk of the head and chest in a frontal collision were investigated using four elderly human models of different sex and size and three restraint systems with different force balances of the shoulder belt and DAB. Even when a restraint system with the same specifications was used, differences in shoulder-belt contact force and the number of rib fractures were observed depending on the body type of the occupant. As shown in the equation in Fig. 11, the contact force applied to the chest from the shoulder belt is proportional to the tension of the belt and the cosine component of the belt wrapping angle. The contact force from the shoulder belt increased while the belt tension was kept constant by the load limiter. This is because the belt wrapping angle decreases as the upper body moves forward. Therefore, it is presumed that the difference in the amount of the chest forward displacement due to the difference in occupant body type was the main cause of the difference in the belt contact force and the number of fractures.

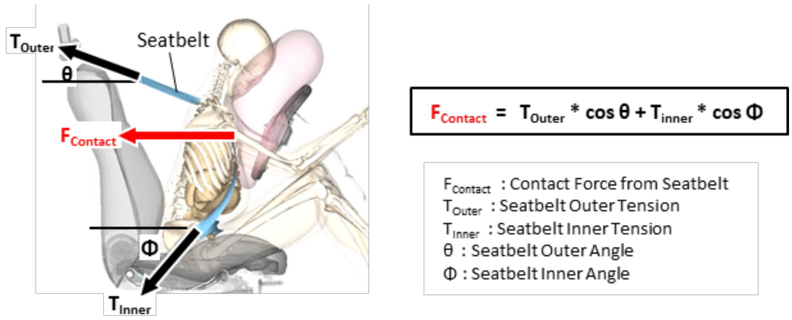

Fig. 11. Relationship between seatbelt contact force and tension.

The small female AF05 model had fewer chest fractures than midsize male AM50 model. AF05 had lower body height and smaller bone cross-sectional area but had lighter weight and forward seating position compared to AM50, which increased the initial restraint force of DAB. As a result, the forward movement of the chest was completed before the contact force of the shoulder belt increased. On the other hand, the overweight female had more fractures than the AM50. Overweight female had lower stature and smaller bone cross-sectional area, but had similar weight compared to AM50. Therefore, the belt contact force applied was almost the same level as AM50. Furthermore, the change in shoulder-belt path due to the large abdominal circumference might also contribute to the fracture. Figure 12 shows the positional relationship between the ribs and the shoulder belt after the seat-belt pretensioner was activated in AM50 and overweight female. In AM50, the buckle moved laterally after the pretensioner was activated, and the belt path moved inward. As a result, the belt hung on the costal cartilage, which was easy to stretch, and the fractures were concentrated around the left upper rib. On the other hand, in overweight female the width of the waist was larger than that of AM50, which reduced the movement of the buckle and the change in the belt path was small. As a result, the belt hung on the right-side ribs and the number of fractures increased. The large male AM95 occupant had more fractures than the AM50. AM95 has a larger bone cross-sectional area but is heavier than AM50. Furthermore, because the seating position was rearward, the chest restraint by the DAB was delayed and the contact force from shoulder belt increased.

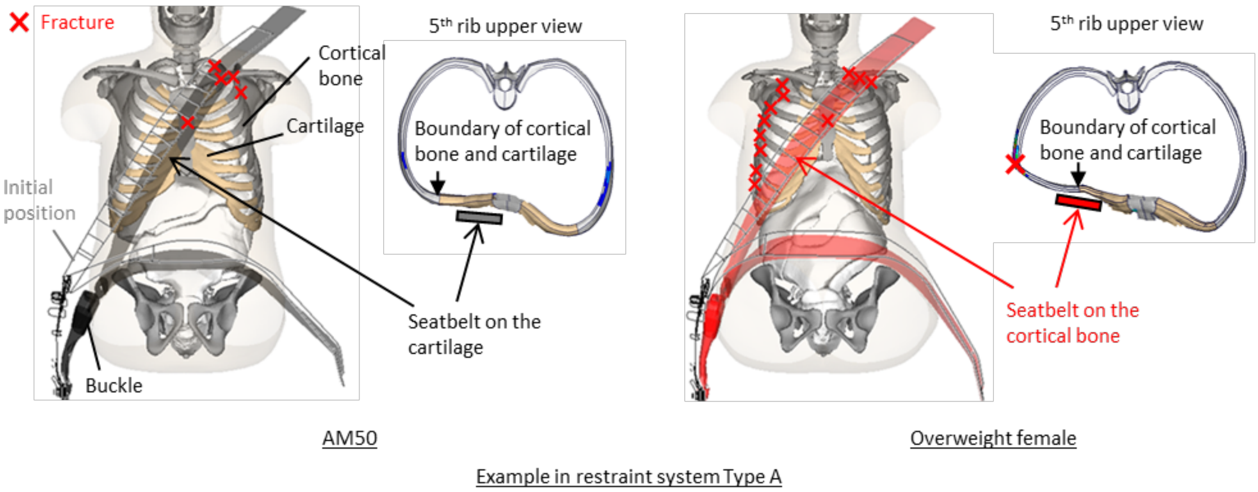

Fig. 12. Positional relationship between shoulder belt and ribcage.

Although the condition of the chest restraint was different for each body type, it was observed that the higher the BMI of the occupants, the higher the number of rib fractures, as shown in Fig. 13. The results indicated that the risk of chest injury was more affected by BMI than by sex in the driver's seat, where the seating position and posture are almost determined by the body height. The number of fractures decreased in the order of restraint devices Type A, B and C. Decreasing the seat-belt tension helps reduce the risk of rib fractures, but could increase the risk of head contact with the steering wheel. In addition to the reduction of the belt tension, the early restraint by the DAB might help prevent the bottoming out of the head and help reduce the chest displacement and the risk of rib fracture. However, the increase in the deployment height of the DAB conflicts with the risk of injury to nearby occupants, so further consideration is required for general conclusion of restraint concept.

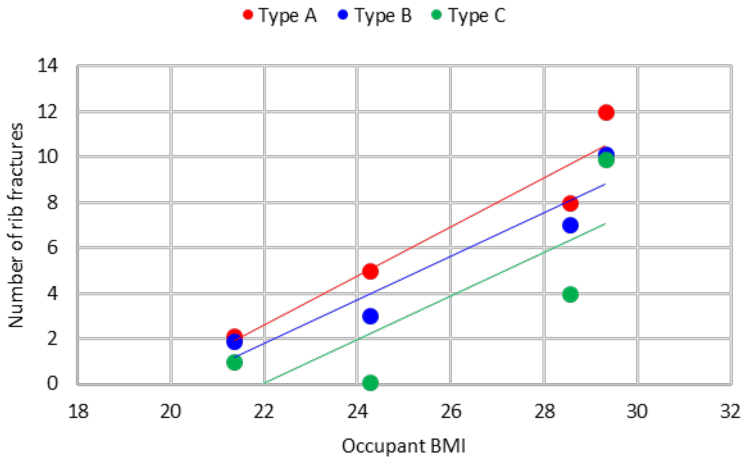

Fig. 13. Relationship between occupant BMI and number of chest fractures.

V. LIMITATIONS

This study assumed a particular sitting posture and position for each occupant model, but of course this may vary among individuals and in specific situations. Interaction with restraint systems is also influenced by such factors. The occupant models used in this study assume a particular geometry and material characteristics, but do contain a large amount of variation. Individual differences in the degree of injury are also considered to be large.

VI. CONCLUSIONS

Human body models of elderly drivers were generated by changing the rib characteristics of the non-elderly (THUMS Version 4.1) occupant model to those of 70yo. Frontal collision simulations in driver's seat were performed using the elderly models. Compared to the midsize male AM50 occupant, the small female occupant AF05 had fewer rib fractures, and the large male AM95 and overweight female had more fractures. It appears that, pending more investigation, it was found that the higher the BMI of the occupant, the greater number of fractures. The lower seat-belt load limiter reduced the contact force from the shoulder belt to the chest and decreased the number of rib fractures. However, the forward displacement of the head increased, and the possibility of secondary collision also increased. The study results indicated that the combination of low load limiter and early airbag constraint was effective to lower rib fracture risk for elderly occupants with various body types. In this study, the simulations were performed in the driver's seat, where the seating position of the occupant is almost determined by the body height. However, the patterns pertaining in the passenger or rear seats might be different from those of the driver's seat, so further research is required.

VII. REFERENCES

[1] National Police Agency (Japan). *Annual Report on Number of fatalities in traffic accidents in 2020* (in Japanese), Internet: https://www.npa.go.jp/publications/statistics/koutsuu/toukeihyo.html, accessed 4 January 2021.

[2] United Nations Economic Commission for Europe (ENECE). Persons Killed or Injured in Road Traffic Accidents (1994-2018), Internet: https://w3.unece.org/PXWeb/en.

[3] Tominaga, S., Nishimoto, T., Motomura, T., Mashiko, K., Sakamoto, Y. (2012) Analysis of Thoracoabdominal Injury based on Japan Trauma Data Bank and In-depth Accident Study. *Transactions of Society of Automotive Engineers of Japan*, **43**(2): pp.269-274.

[4] Adams, M., Bass, C. (2021) The Effect of Rib Fracture Patterns in the Obese. *Proceedings of IRCOBI Conference*, 2021.

[5] Ejima, S., Holcombe, S., *et al*. (2017) Female vs. Male Relative Fatality Risk in Fatal Crashes. *Proceedings of IRCOBI Conference*, 2017, Antwerp, Belgium.

[6] Crandell, J., Forman, J., Joodaki, H. (2015) First Generation Obese ATD (FGOA). *Proceedings of the 24st ESV Conference*, 2015, Gothenburg, Sweden.

[7] Takahira, Y., Akima, S., Kusuhara, Y., Tanase, N., Kitagawa, Y. (2021) Cross-Sectional Analysis of Rib Fracture Mechanism of Elderly Occupant in Frontal Collision using THUMS. *Proceedings of IRCOBI Conference*, 2021.
[8] Holcombe, S., Brown, E., Wang, S. (2020) Building a better rib. *Proceedings of the JSAE Annual Congress (Spring),* 2020.
[9] Holcombe, S., Wang, S., Grotberg, B. (2017) The effect of age and demographics on rib shape. *Journal of Anatomy,* **12632**: pp.229–247.
[10] Watanabe, R., Miyazaki, H., Kitagawa, Y., Yasuki, T. (2012) Research of the relationship of pedestrian Injury to collision speed, car-type, impact location and pedestrian sizes using human FE model (THUMS Version 4). *Stapp Car Crash Journal*, **561**: pp.269-321.
[11] Shigeta, K., Kitagawa, Y., Yasuki, T. (2009) Development of next generation human FE model capable of organ injury prediction. *Proceedings of the 21st ESV Conference*, 2009, Stuttgart, Germany.
[12] Kitagawa, Y., Yasuki, T. (2013) Correlation among seatbelt load, chest deflection, rib fracture and internal organ strain in frontal collisions with human body finite element models. *Proceedings of IRCOBI Conference*, 2013, Gothenburg, Sweden.
[13] Kitagawa, Y., Hayashi, S., Yamada, K., Gotoh, M. (2017) Occupant kinematics in simulated autonomous driving vehicle collisions, direction and angle. *Stapp Car Crash Journal*, **61**: pp.101-155.

VIII. APPENDIX

TABLE A-I
SIMULATION RESULTS OF THOR AM50 INJURY INDEX IN 56 KM/H FRONTAL COLLISION SLED

Body Reagion	Injury Index			Type A	Type B	Type C
Head	HIC15			293	329	333
Neck	Nij			0.508	0.535	0.486
Chest	Resultant Deflection	Left Upr	mm	22.3	24.6	25.3
		Left Lwr	mm	9.9	8.5	9.2
		Right Upr	mm	42.4	41.3	44.7
		Right Lwr	mm	34.5	27.7	34.6
Abdomen	X-axis Deflection	Left	mm	66.4	69.4	67
		Right	mm	65.1	73	66.3
KTH	Acetabulum F-res	Left Upr	kN	2.215	2.764	2.459
		Left Lwr	kN	1.835	2.22	1.988
	Femur Fz	Right Upr	kN	2.851	2.838	2.816
		Right Lwr	kN	3.095	3.277	3.169
Lower Leg	Tibia Fz	Left Upr	kN	1.811	1.862	2.076
		Left Lwr	kN	1.937	1.913	1.929
		Right Upr	kN	2.242	2.251	1.976
		Right Lwr	kN	3.085	3.125	2.896
	Tibia Bending M_res	Left Upr	Nm	85.1	71.3	81.3
		Left Lwr	Nm	30	25.8	35
		Right Upr	Nm	63.8	76.6	85.5
		Right Lwr	Nm	30.7	29.3	32.9